九州大学大学院総合理工学府報告
第 43 巻 第 2 号 37-41 頁 令和 4 年 2 月

Engineering Sciences Reports, Kyushu University
Vol. 43, No. 2, pp. 37-41, FEB, 2022

Spectroscopic Study for UV Irradiation Effect on Adsorption State of Volatile Aldehyde at Single Crystalline ZnO Nanowire Surface

Wenjun LI[*1,2] Kazuki NAGASHIMA[*2,3†] Chen WANG[*4]
Hideto YOSHIDA[*5] Takuro HOSOMI[*2,3] Tsunaki TAKAHASHI[*2,3]
Wataru TANAKA[*2] Masaki KANAI[*6] and Takeshi YANAGIDA[*2,6†]
[†]E-mail of corresponding author: kazu-n@g.ecc.u-tokyo.ac.jp, yanagida@cm.kyushu-u.ac.jp

(Received January 20, 2022, accepted January 26, 2022)

Ultraviolet (UV) irradiation is a promising approach for enhancing a sensing response in metal oxide-based molecular sensor, however, its substantial impact on the molecular-to-surface interaction at sensor surface is poorly understood. In this study, we investigated the UV irradiation effect on adsorption state of volatile aldehyde at single crystalline zinc oxide (ZnO) nanowire surface by Fourier transform-infrared spectroscopy (FT-IR). A C9 aliphatic aldehyde, nonanal, was employed as an analyte. We found that oxidation of adsorbed nonanal was significantly promoted by the UV irradiation. A wavelength dependence implied that the photogenerated carriers play a crucial role in the enhanced oxidation. Our finding would be beneficial for designing the performances of metal oxide nanowire-based molecular sensing devices.

Key words: *Single crystalline, ZnO, nanowires, volatile molecule, aldehyde, nonanal, FT-IR, adsorption, UV irradiation, molecular sensing*

1. Introduction

Metal oxide nanowires have attracted considerable research interest for molecular sensor applications due to their unique structural properties, variety of chemical reactions, and material robustness in harsh environments.[1-3] To date, various nanowire materials have been intensively investigated with their surface treatments/modifications and many excellent sensor properties have been successfully demonstrated.[4-11] On the other hand, the interactions between nanomaterial surfaces and analyte molecules have not been understood comprehensively, which had limited the design of sensing performance. To overcome this issue, many efforts have recently been devoted to the understanding of molecule-to-surface interactions at sensor surface by using spectroscopic techniques.[12-15] We previously investigated the adsorption states of volatile molecules at the surfaces of metal oxide nanowires (i.e., zinc oxide (ZnO) nanowires and tungsten oxide (WO_3) nanowires) by infrared (IR) spectroscopy, and various adsorption states and chemical transformations of adsorbed molecules were revealed.[16-20] Furthermore, according to the acquired knowledge, we modified the nanowire surfaces and successfully achieved the improved sensing properties.[18-20] As proven in these studies, understanding the molecule-to-surface interactions at metal oxide nanowire surfaces is of crucial importance for designing the performance of nanowire-based molecular sensors.

Among various features of molecular sensors, sensitivity (i.e., amplitude of sensing response) is the most important one for detecting analyte molecules at extremely low concentration.

*1 Department of Molecular and Material Sciences, Interdisciplinary Graduate School of Engineering Sciences, Kyushu University, Graduate Student
*2 Department of Applied Chemistry, Graduate School of Engineering, The University of Tokyo
*3 Japan Science and Technology Agency, PRESTO
*4 Department of Electronic and Computer Engineering, School of Engineering, The Hong Kong University of Science and Technology
*5 Nanoscience and Nanotechnology Center, The Institute of Scientific and Industrial Research, Osaka University
*6 Division of Integrated Materials, Institute for Materials Chemistry and Engineering, Kyushu University

Such demand emerges for example in breath sensing-based disease diagnosis.[21,22] As well as structural control and surface catalyst decoration,[23-26] ultraviolet (UV) irradiation is known as a promising approach for enhancing the sensitivity of metal oxide-based molecular sensor.[27-29] The substantial impact of UV irradiation on molecule-to-surface interaction at sensor surface is, however, poorly understood. These backgrounds motivated us to conduct the spectroscopic study for the UV irradiation effect on molecule-to-surface interactions.

In this study, we investigated the UV irradiation effect on adsorption state of volatile aldehyde at single crystalline ZnO nanowire surface by Fourier transform-infrared spectroscopy (FT-IR), as schematically illustrated in Fig.1. C9 aliphatic aldehyde of nonanal, i.e., a biomarker molecule of lung cancer in exhaled air,[30] was used as an analyte. We found that the oxidation of adsorbed nonanal was significantly promoted by the UV irradiation. The oxidation mechanism was discussed in consideration of its wavelength dependence.

2. Experimental

2.1 Preparation of ZnO Nanowires

ZnO nanowires were synthesized via a seed-assisted hydrothermal synthesis.[31-38] A Si wafer coated with ZnO seed layer was used as a substrate for the nanowire growth. Prior to the hydrothermal synthesis, a 5 nm-thick ZnO seed layer was deposited on Si wafer with a 1 nm-thick Ti adhesive layer by radio frequency (RF) sputtering with the RF power of 50 W and the argon pressure of 0.3 Pa. For the ZnO nanowire growth, 25 mM zinc nitrate hexahydrate ($Zn(NO_3)_2 \cdot 6H_2O$), 25 mM hexamethylenetetramine (HMTA), 2.5 mM of polyethyleneimine (PEI) and 3 mL of $NH_3 \cdot H_2O$ (27% in water) were dissolved in 100 mL deionized (DI) water in this order by stirring at room temperature. Then the ZnO seed layer-coated substrate was immersed into the solution in an up-side-down manner. The hydrothermal synthesis was conducted at 95 °C for 10 h. As-grown sample was rinsed in DI water, dried by air blow, and annealed at 600 °C for 1 h in air. The morphology and the crystal structure of synthesized ZnO nanowires were characterized by field emission scanning electron microscopy (FESEM) at an accelerating voltage of 15 kV, transmission electron microscopy (TEM) at that of 200 kV, and X-ray diffractometry (XRD) measurement.

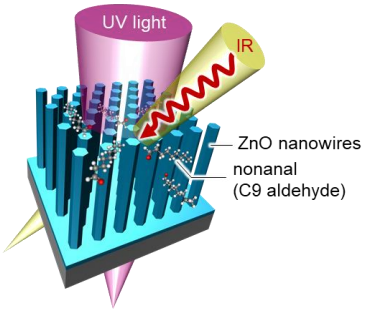

Fig.1 Schematic illustration of the spectroscopic study for the UV irradiation effect on the molecular adsorption state at metal oxide nanowire surface.

2.2 Molecular Adsorption and UV Irradiation

For examining the UV irradiation effect on the molecular adsorption state, 2 μL liquid concentrate of nonanal (C9 aliphatic aldehyde), was dropped on a ZnO nanowires-grown rectangular-shaped substrate (size; 15 mm×15 mm) and dried by nitrogen blow to remove the excess nonanal. Then UV light with three different wavelengths (λ = 260 nm, 300 nm, and 350 nm) was irradiated to the nonanal-adsorbed ZnO nanowires with varying the irradiation time for 0–40 min. We performed FT-IR for the nonanal-adsorbed ZnO nanowires after each UV irradiation time. All the experiments were performed at room temperature in air condition.

3. Results & Discussion

3.1 Characterization of ZnO Nanowires

Figs.2(a) and (b) show the FESEM images of ZnO nanowires grown on the substrate, which correspond to the 45°-tilted view and the cross-sectional view, respectively. The ZnO nanowires were grown almost perpendicular to the substrate. The length and the diameter of ZnO nanowires were ~6.5 μm and ~80-120 nm, respectively. Fig.2(c) shows the TEM image of single ZnO nanowire. The nanowire was well-crystalline, and the surface was microscopically smooth. Fig.2(d) shows the selected area electron diffraction (SAED) pattern of the ZnO nanowire in Fig.2(c). The single crystalline nature and the [0001]-oriented growth direction of the synthesized ZnO nanowire were identified in the SAED pattern. The [0001]-oriented growth

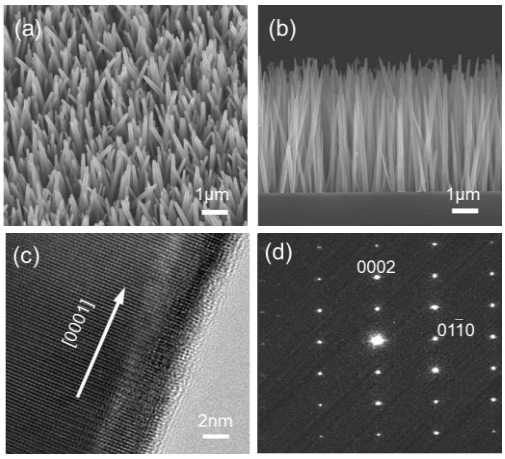

Fig.2 (a,b) FESEM images of ZnO nanowires: (a) 45°-tilted view and (b) cross-sectional view. (c) TEM image and (d) SAED pattern of a single ZnO nanowire.

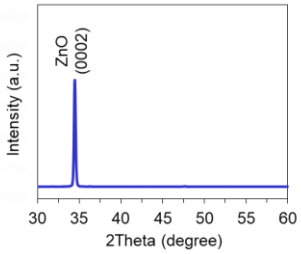

Fig.3 XRD pattern of ZnO nanowires grown on a substrate.

of ZnO nanowire originated from i) the minimization of total interfacial energy during the nanowire growth[31-34] and ii) the (10-10) plane-selective capping feature of PEI.[39] To statistically analyze the crystal structure of synthesized ZnO nanowires, the XRD measurement was conducted, and the result is shown in Fig.3, In the XRD pattern, the (0002) peak was seen at 34.42° and no other peaks were observable. The results confirmed the single crystalline nature and the [0001]-oriented growth direction of ZnO nanowires as consistent with TEM and SAED results. The diffraction peak could be indexed to wurtzite ZnO (JCPDS Card No. 36-1451). Thus, we successfully synthesized the single crystalline ZnO nanowire array with well-defined structure, which serves as a platform to investigate the UV irradiation effect on the molecular adsorption state.

3.2 UV Irradiation Effect on Nonanal Adsorption State at ZnO Nanowire Surface

The UV irradiation effect on the molecular adsorption state was investigated by FT-IR

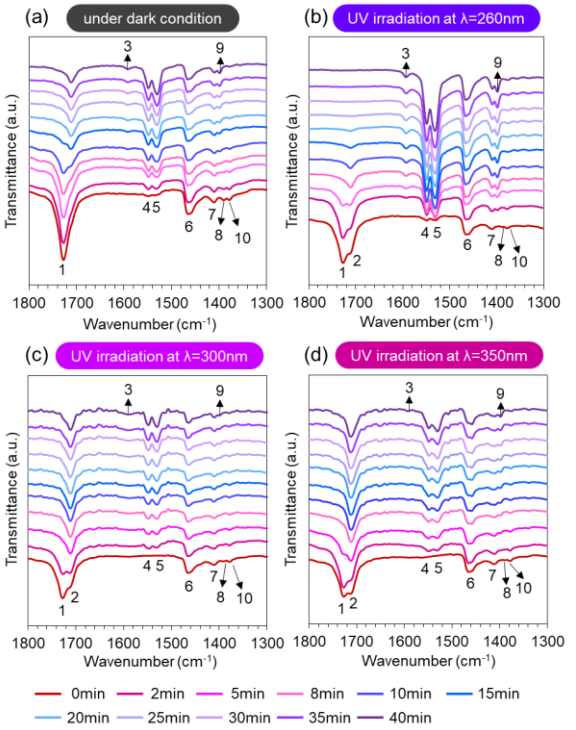

Fig.4 Time evolution FT-IR spectra of nonanal adsorbed on the ZnO nanowires (a) under dark condition, (b) with UV irradiation at λ = 260 nm, (c) with UV irradiation at λ = 300 nm, and (d) with UV irradiation at λ = 350 nm, respectively.

using nonanal as an analyte molecule. Fig.4(a) shows the time evolution FT-IR spectra of nonanal adsorbed on the ZnO nanowires under no UV irradiation (i.e., a dark condition). In the spectra, several peaks, which can be assigned as the vibration modes of ν(C=O), ν(COO), δ(CH_2), δ(CH_3) and δ(CH), were observed (as listed in Table 1).[40] Complex peak patterns of ν(COO) arise from various adsorption structures such as bridging, bidentate and monodentate.[41] Extended UV

Table 1 List of observed IR peaks

peak no.	wavenumber (cm^{-1})	vibration mode
1	1727	ν_s(C=O)
2	1711	
3	1592	ν_{as}(COO)
4	1549	
5	1530	
6	1467	δ(CH_2/CH_3)
7	1410	δ(CH_2/CH_3)
8	1390	δ(CH)
9	1399	ν_s(COO)
10	1378	δ_s(CH_3)

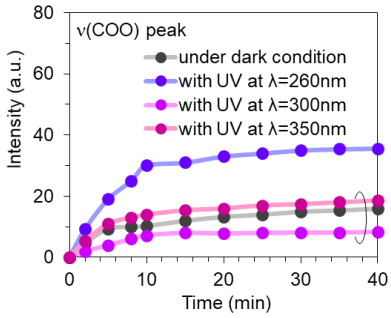

Fig.5 The variations of peak intensity of ν(COO) under the different UV irradiation conditions.

irradiation time resulted in decrease in the intensity of ν(C=O) peaks and concomitant increase in that of the ν(COO) peaks became larger. The result indicated that the adsorbed nonanal was gradually oxidized at ZnO nanowire surface, and unreacted nonanal and oxidized nonanal coexist even after 40 min.

Fig.4(b) shows the time evolution FT-IR spectra of nonanal adsorbed on the ZnO nanowires under UV irradiation at the wavelength of λ = 260 nm. We found that the ν(C=O) peaks fully disappeared after 30 min of UV irradiation and the intensity of ν(COO) peaks remarkably increased. In addition, no other variations in FT-IR spectra were observed by the UV irradiation. These results implied that the UV irradiation promoted the oxidation of surface-adsorbed nonanal.

3.3 Wavelength Dependence of UV Irradiation Effect

To gain an in-depth understanding as to the promoted oxidation of adsorbed nonanal, we next investigated the wavelength dependence of UV irradiation. Figs.4(c) and Fig.4(d) show the time evolution FT-IR spectra of adsorbed nonanal when performing the UV irradiation at the wavelength of λ= 300 nm and λ= 350 nm, respectively. Contrary to the result of UV irradiation at λ= 260 nm, the ν(C=O) peaks remained even after 40 min for both cases. Also, the increase of ν(COO) peak intensity was not so remarkable. Note that the initial states of nonanal in Figs.4(a)-(d) were largely different, which originated from the difficulty to fully remove the excess nonanal from the nanowire surface during the sample preparation. Nevertheless, the observed UV irradiation effect and its wavelength dependence cannot be consistently interpreted by the difference of initial states. To directly compare the progress of nonanal oxidation at different UV irradiation conditions, the peak intensity of ν(COO) was plotted as a function of UV irradiation time in Fig.5. For this comparison, the ν(COO) peak at 1549 cm^{-1} was used. The promoted oxidation of adsorbed nonanal was seen only at λ= 260 nm, but not at λ= 300 nm and λ= 350 nm. Specifically, the intensity of ν(COO) peak for the UV irradiation at λ= 260 nm was about 2 times higher compared with those for the dark condition and the UV irradiation at other wavelengths. Thus, these results indicated that the UV irradiation at λ= 260 nm significantly promoted the oxidation of adsorbed nonanal beyond the limit at the given temperature condition. Because the sensing of volatile organic compounds closely correlates with the oxidation of molecules,[42] the enhancement of sensitivity would be expected in ZnO nanowire-based nonanal sensing by the UV irradiation at λ= 260 nm, which is planned as a future work.

3.4 Discussion of UV Irradiation Effect

Here we discuss why the oxidation of nonanal was promoted by the UV irradiation. According to the wavelength dependence, we considered that the photogenerated carriers in ZnO nanowires strongly contributed to the oxidation of nonanal. Because ZnO has a wide bandgap of *ca.* 3.3 eV,[43] photogenerated carriers are produced by UV irradiation and its quantum yield tends to become higher at shorter wavelength. The photogenerated electrons in conduction band combine with surface-adsorbed oxygen to form superoxide ions and the photogenerated holes in valence band combine with surface-adsorbed water molecules to form hydroxyl radicals.[44,45] Such photogenerated species are reactive and thus might promote the oxidation of adsorbed nonanal.

4. Summary and Conclusion

We investigated the UV irradiation effect on the adsorption state of nonanal at single crystalline ZnO nanowire surface by FT-IR. We found that oxidation of adsorbed nonanal was significantly promoted by the UV irradiation. A wavelength dependence showed that the UV irradiation at λ= 260 nm enhanced the oxidation beyond the limit at the given temperature condition. We discussed the UV irradiation-induced promotion of oxidation via the photogenerated carriers. Our finding in this study would lead to the in-depth

understanding of the molecular sensing mechanism and thus be beneficial for designing the performances of metal oxide nanowire sensors.

Acknowledgments

This work was supported by KAKENHI (No. JP21K18868, JP18H05243) and PRESTO Program (No. JPMJPR19J7) of Japan Science and Technology Corporation (JST). K.N. acknowledges JACI. This work was partly supported by the Cooperative Research Programs of “Dynamic Alliance for Open Innovation Bridging Human, Environment and Materials in Network Joint Research Center for Materials and Devices”, “Network Joint Research Center for Materials and Devices”.

References

1) Z. Zhou et al., J. Mater. Chem. C 7, 202 (2019).
2) G. Zhang et al., Analyst 146, 6684 (2021).
3) H. Zeng et al., Chemosensors 9, 41 (2021).
4) S.-Y. Jeong et al., Adv. Mater. 32, 2002075 (2020).
5) M.-S. Yao et al., Adv. Mater. 28, 5229 (2016).
6) M. Singh et al., J. Mater. Chem. A in press (2022) DOI：10.1039/d1ta09290a.
7) M. Singh et al., Adv. Funct. Mater. 30, 2003217 (2020)
8) R. Yamaguchi et al., Langmuir 37, 5172 (2021).
9) K. Nakamura et al., ACS Omega 7, 1462 (2022).
10) G. Zheng et al., Nat. Biotechnol. 23, 1294 (2005).
11) T. Shimada et al., Lab Chip 18, 3225 (2018).
12) S. Sänze et al., Angew. Chem. Int. Ed. 52, 3607 (2013).
13) A.-K. Elger et al., Angew. Chem. Int. Ed. 58, 15057 (2019).
14) A.-K. Elger et al., ACS Sens. 4, 1497 (2019).
15) A. Sharma et al., J. Mater. Chem. A 9, 18175 (2021).
16) C. Wang et al., Nano Lett. 19, 2443 (2019).
17) K. Nakamura et al., ACS Appl. Mater. Interfaces 11, 40260 (2019).
18) C. Wang et al., ACS Appl. Mater. Interfaces 12, 44265 (2020).
19) J. Liu et al., Chem. Sci. 12, 5073 (2021).
20) G. Zhang et al., J. Mater. Chem. A 9, 5815 (2021).
21) S.-J. Kim et al., Acc. Chem. Res. 50, 1587 (2017).
22) G. Konvalina et al., Acc. Chem. Res. 47, 66 (2014).
23) S. Nekita et al., ACS Appl. Nano Mater. 3, 10252 (2020).
24) G. Zhang et al., Nanoscale 12, 9058 (2020).
25) X. Zou et al., Nano Lett. 13, 3287 (2013).
26) N. M. Vuong et al., Sci. Rep. 6, 26736 (2016).
27) H.-S. Woo et al., Sensors 16, 1531 (2016).
28) L. Zhu et al., Sens. Actuators A 267, 242 (2017).
29) A. Mirzaei et al., Chemosensors 7, 56 (2019).
30) P. Fuchs et al., Int. J. Cancer 126, 2663 (2010).
31) Y. He et al., J. Phys. Chem. C 117, 1197 (2013).
32) Y. Akihiro et al., ACS Omega 4, 8299 (2019).
33) D. Sakai et al., Sci. Rep. 9, 14160 (2019).
34) X. Zhao et al., Nano Lett. 20, 599 (2020).
35) J. Liu et al., Chem. Lett. 49, 1220 (2020).
36) J. Liu et al., Commun. Mater. 1, 58 (2020).
37) Q. Liu et al., J. Phys. Chem. C 124, 20563 (2020).
38) R. Kamei et al., ACS Appl. Mater. Interfaces 13, 16812 (2021).
39) R. Parize et al., ACS Omega 3, 12457 (2018).
40) P. Larkin, Infrared and Raman spectroscopy; principles and spectral interpretation. Amsterdam Elsevier (2011).
41) C. C. R. Sutton et al., Chem. Eur. J. 21, 6801 (2015).
42) T. Lin et al., Sensors 19, 233 (2019).
43) B. Wei et al., Nano Lett. 12, 4595 (2012).
44) W. He et al., J. Am. Chem. Soc. 136, 750 (2014).
45) Y. Li et al., Int. J. Mol. Sci. 21, 8836 (2020).